express
polymer letters

Research article

High gas barrier properties of novel urea-carbamate functionalized polydimethylsiloxane composites star-crosslinked by graphene oxide

Yuwei Gu[1], Lijun Chu[1], Quanxiao Dong[2,3], Peng Qiu[2,3], Stephen Jerrams[4], Shui Hu[1], Shipeng Wen[1] ![ORCID]

[1]State Key Laboratory of Organic-Inorganic Composites, Beijing University of Chemical Technology, 100029 Beijing, China
[2]Hebei Tieke Yichen New Materials Technology Co.Ltd, Shijiazhuang, 052160 Hebei, China
[3]Railway Engineering Research Institute, China Academy of Railway Sciences Corporation Limited, 100081 Beijing, China
[4]Technological University Dublin, D01 K8222 Dublin, Ireland

Abstract. Polydimethylsiloxane has the characteristics of low-temperature flexibility and excellent aging resistance. However, high molecule mobility and weak interactions between PDMS molecules result in poor mechanical strength and deficient gas barrier properties of PDMS composites. Herein, diamino-polydimethylsiloxane (PDMS) was reacted with 4,4′-diphenylmethane diisocyanate (MDI) and 1,4-butanediol (BDO) to form urea-carbamate functionalized PDMS (MDI-PDMS-BDO) with different hard segment contents. Furthermore, the modified graphene oxide (iGO) was obtained by the reaction between graphene oxide (GO) and MDI. iGO was further introduced into the functionalized PDMS to prepare iGO/urethane-urea functionalized PDMS composites (iGO/MDI-PDMS-BDO). An ordered structure was formed by the hard segments of the MDI-PDMS-BDO functionalized PDMS. A strong urea-based interface was also obtained between iGO and functionalized PDMS. iGO became the cross-linking center in the iGO/MDI-PDMS-BDO composites. Due to the ordered structure of hard segments and the iGO network formed in the PDMS composite with only 0.07 wt% iGO, the tensile strength and gas barrier properties of the iGO/MDI-PDMS-BDO composite were increased by 18 times and 64.27%, respectively, compared with pure PDMS.

Keywords: polydimethylsiloxane, carbamate-urea, graphene oxide, gas barrier property

1. Introduction

High gas barrier materials that are used in confined spaces, such as space stations and high-clean laboratories, require not only good gas barrier properties but also low odor and environmentally friendly characteristics. At present, the rubber matrices used for most airtight materials are primarily natural rubber (NR), nitrile butadiene rubber (NBR), and isobutylene isoprene rubber (IIR). These rubber composites containing nanofillers have high air tightness. However, the various organic functional additives, including antioxidant and vulcanization additives, emit unpleasant odors and are harmful to human health. Therefore, it is imperative to develop a rubber composite with high air tightness and environmentally friendly properties [1–4].

At present, a relatively environmentally friendly rubber is polydimethylsiloxane (PDMS), possessing a main –Si–O– chain [5–7]. PDMS exhibits acceptable softness over a wide temperature range. Moreover,

---

*Corresponding author, e-mail: wensp@mail.buct.edu.cn

the glass transition temperature of PDMS is lower than –100 °C. It has very good aging resistance and is chemically inert [8, 9]. Therefore, no antioxidants are required in PDMS composites, making them candidates for environmentally-friendly materials. However, the disadvantage of PDMS is that the interaction force between molecules is too weak, leading to large free volumes in the PDMS composite. Hence, external gas and liquid small molecules easily penetrate into the PDMS matrix, resulting in poor mechanical and barrier properties [10]. Therefore, the improvement of gas barrier properties of PDMS presents a great challenge.

Two approaches can be adopted for improving the low gas barrier property of PDMS. First, polar groups can be introduced into the PDMS chains to increase the interaction between adjacent PDMS chains [11]. Also, soft and hard phase coexisting structures could be obtained by introducing polar groups into the molecular chain of PDMS [12, 13]. Liu *et al.* [14] established a new cross-linking system acting on the urea group with an organic silicon polyurea block copolymer as the raw material. The increase in the polyurea units enhanced the degree of hydrogen bond binding and microphase separation, leading to an increase in hardness, tensile strength and elongation at break. Zang *et al.* [15] synthesized carboxyl-grafted polymethylvinylsiloxane (PMVS-COOH) and amino-grafted polydimethylsiloxane (PDMS-NH_2) and mixed them to form a hydrogen-bonded cross-linked supramolecular PDMS matrix (SiR-SN). SiR-SN formed by hydrogen bonding cross-linking of polar groups played a great role in improving the self-healing properties and recyclability of the composites. However, few investigations of modified PDMS focused on gas barrier properties.

Second, particles with a lamellar structure can be introduced into PDMS to form complex filler networks, thereby inhibiting and lengthening the path of gas molecules through and consequently improving air tightness. Compared with spherical particles and fibers, graphene oxide (GO) more readily forms a filler network that hinders the penetration of gas molecules due to its unique two-dimensional lamellar structure and large aspect ratio [16, 17]. The oxygen-containing functional groups on the surface of GO can react with the polymer matrix through covalent bonds or non-covalent bonds to form strong interfaces, and reduce the volume between GO sheets and the polymer molecular chain [18]. Bernard *et al.* [19]

studied the effect of the GO content on the properties of waterborne polyurethane (WPU) coatings. The oxygen permeability was decreased by 7 times under a high GO content due to the large inter-layer spacing in GO facilitated the intercalation of polar monomers, oligomers and small molecules into these locations. Zheng *et al.* [20] prepared GO/butyl rubber (GO/IIR) composites by the green latex compounding method. There was a strong interfacial interaction between GO and IIR chains. Compared with IIR, the tear and tensile strength of GO/IIR composites were increased by 44 and 102%, respectively.

In this research, to introduce polar groups into PDMS, a urea group and carbamate group were reacted with diamino-terminated polydimethylsiloxane (PDMS) to form urea-carbamate-based functionalized PDMS (MDI-PDMS-BDO). The addition of a urethane group reduced the phase separation between the urea group and PDMS. Furthermore, modified GO (iGO) was covalently linked with polyurea-carbamate chains to form iGO/MDI-PDMS-BDO composites. The iGO aced as the cross-linking center and formed a GO filler network. The enhanced MDI-PDMS-BDO molecule interaction and GO filler network efficiently hindered the gas penetration and finally improved the gas barrier properties.

2. Experimental section
2.1. Materials
Graphene oxide (GO) was made in the laboratory according to the improved Hummers method [21]. Diamino-polydimethylsiloxane (PDMS, M_n = 3000) was purchased from Gelest Inc. (Germany). 4,4′-diphenylmethane diisocyanate (MDI) and 1,4-butanediol (BDO) were purchased from Shanghai Aladdin Biochemical Technology Co., Ltd. (China). *N,N*-dimethylformamide (DMF), dichloromethane, tetrahydrofuran, methanol and other organic solvents were purchased from the Beijing Chemical Plant (China).

2.2. Characterization
Fourier-transformed infrared spectroscopy (FTIR) was used to confirm the success synthesis of samples by employing a Tensor 27 infrared spectrometer (Bruker, Germany). The urea-carbamate modified PDMS and iGO/MDI-PDMS-BDO composites were dissolved in tetrahydrofuran (THF) and dropped the film on KBr. Then, the samples were tested after drying. The test wavenumber range was 400-4000 cm^{-1}. X-ray diffraction (XRD, Rigaku Corporation, Japan)

was used to characterise the ordered structure of the iGO/MDI-PDMS-BDO composites. During the test, the diffraction source was Cu K_α. The test angle was over the range of 5–90°, and the scanning rate was 5°/min. The differential scanning calorimeter (DSC) was used to characterize the T_g of the samples by employing the Stare system DSC thermal analyzer (Mettler-Toledo International, Inc., Switzerland). The test temperature was in the range from –140 to 100 °C, and the heating rate was 10 °C/min. Gas barrier properties were tested using a differential pressure gas permeameter (VAC-V2, Jinan Labthink Electromechanical Technology Co., Ltd., China). The samples were approximately 1 mm thick and 8 cm in diameter. The test temperature was 23 °C. The micromorphology of functional silicone rubber and composites was characterised using atomic force microscopy (AFM, Multimode 8, Bruker, Germany). The static mechanical properties of silicone rubber and iGO/urea functionalised silicone rubber composites were tested using a tensile machine (Text-port II, Zwick Roell, Germany) according to ISO 37:2005. The test was carried out using a transducer with a load cell of 20 N. The molecular weight of PDMS was obtained from the gel permeation chromatography (GPC, Agilent 1260, Agilent Technologies Inc., USA). The solvent was tetrahydrofuran, and the concentration of the test samples ranged from 0.01 to 0.05% (w/v). The surface morphologies of iGO/MDI-PDMS-BDO composites were observed by the scanning electron microscope (SEM, Sigma 300, HCarl Zeiss Microscopy GmbH, Germany). The surfaces of the composite were obtained by fracturing the samples under a liquid nitrogen atmosphere and then sprayed with gold particles in a sputter coater. The acceleration voltage was 3 kV, and the working distance was 8–9 mm. A hardness tester (LX-A, Jiangsu Tianhui Testing Machinery Co., Ltd., China) was used to test the hardness of the samples according to ISO 7619:2010. Three samples were tested, and the median value was chosen among the three tested hardness values.

2.3. Preparation of pure PDMS

100 g silicone rubber (SiR) (brand 110-2) and 1 g dicumyl peroxide (DCP) were mixed in a two-roll mill to obtain the masterbatch. The first vulcanization stage was carried out at 160 °C for 12 min on a flat vulcanizing machine. The second vulcanization stage was achieved by placing the samples in an oven at 160 °C for 2 h.

2.4. Preparation of urea/carbamate modified PDMS

The synthetic formulation is shown in Table 1. A certain amount of PDMS and MDI were dissolved in THF to form a uniform solution, respectively. Then, MDI/THF solution was added to the PDMS/THF solution at 0 °C in a nitrogen atmosphere for 8 h to form the prepolymer solution. Afterwards, the chain extender BDO was dissolved in tetrahydrofuran to form a 5% solution and dropwise added to the prepolymer solution. After the reaction, the THF solvent was removed to obtain MDI-PDMS-BDO urea-carbamate functionalized PDMS. The functionalized PDMSs with different hard segment contents were prepared by changing the ratio of MDI:PDMS:BDO according to the method described here. The samples were named as the MDI-PDMS-BDO 1-5, according to the different ratios of PDMS:MDI:BDO shown in Table 1.

2.5. Modification of GO

GO was ultrasonically dispersed in *N,N*-dimethylformamide (DMF) for 30 min to form a 2 mg·ml^{-1} solution. MDI was added and reacted with GO at 80 °C for 10 h in an N$_2$ atmosphere. The unreacted GO was washed away in dichloromethane. After repeating the centrifugal washing for three times, the modified GO (iGO) was further freeze-dried.

2.6. Preparation of iGO/MDI-PDMS-BDO composites

iGO was ultrasonically dispersed in a THF/DMF mixed solution. The sample of MDI-PDMS-BDO 5

Table 1. Synthetic formula of urea-carbamate functionalized SiR.

Sample	PDMS:MDI:BDO [mol]	PDMS-3000 [g]	MDI [g]	BDO [g]
MDI-PDMS-BDO 1	1:2:1	8.36	1.39	0.25
MDI-PDMS-BDO 2	1:3:2	7.63	1.91	0.46
MDI-PDMS-BDO 3	1:4:3	7.02	2.34	0.63
MDI-PDMS-BDO 4	1:5:4	6.51	2.71	0.78
MDI-PDMS-BDO 5	1:6:5	6.06	3.03	0.91

with the high hard segment content was selected as the matrix. iGO solution was added to the MDI-PDMS-BDO 5 solution. After reaction at 60 °C for 8 h in an N_2 atmosphere, the reaction mixture was flocculated in a mixed solution of deionized water and methanol. The samples were washed three times, dried at 60 °C, and then vacuum dried to constant mass. The samples of iGO/MDI-PDMS-BDO composites were named as mass fractions of iGO in composites.

3. Results and discussion
3.1. Characterisation of MDI-modified graphene oxide (iGO)

Figure 1 shows the FTIR spectra of GO before and after modification. The peaks located at 3450, 1068, and 1630 cm^{-1} represent the –OH, C–O–C stretching vibration, and C–OH bending vibration on GO, respectively [22, 23]. The C=O vibration in the carbamate group appeared at 1710 cm^{-1} in the curves for
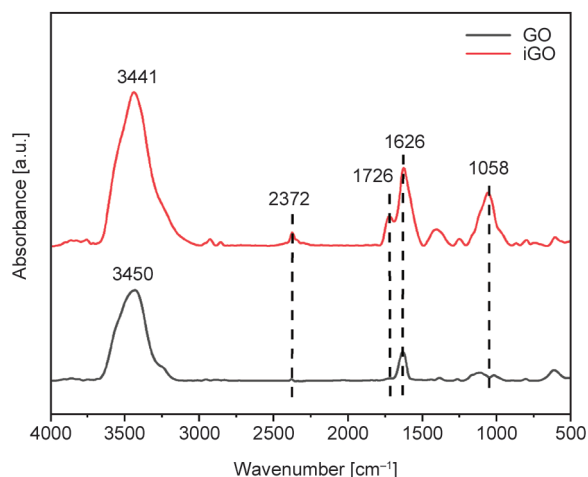

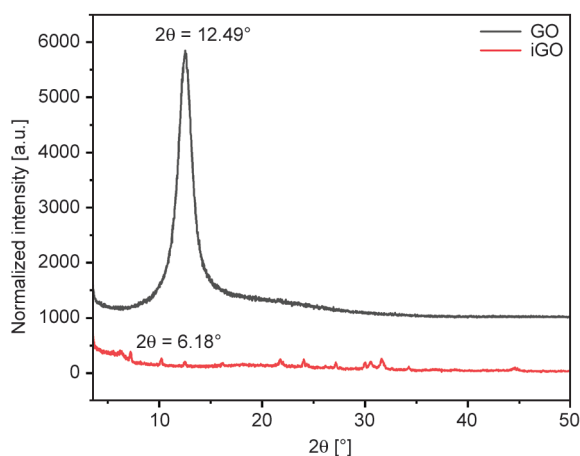**Figure 1.** FTIR spectra of GO and iGO.

Figure 2. XRD patterns of GO and iGO.

iGO, indicating that the isocyanate group in the one end of the MDI successfully reacted with the hydroxyl and carboxyl groups of GO, while the characteristic peak of –NCO still existed at 2265 cm^{-1}, indicating that the other end of the MDI was retained to ensure the subsequent compounding of iGO with urethane-functionalized PDMS.

XRD patterns in Figure 2 shows the diffraction peak of GO appeared at 12.49° [24]. After modification, the intensity of the diffraction peak of iGO became weak and shifted to a small angle, indicating an increase in the the degree of defects and lamellar spacing of GO after modification.

3.2. Synthesis mechanism of graphene oxide/urea-urethane functionalized PDMS composites

To increase the polarity of the PDMS matrix, strong polarity 4,4-diphenylmethane diisocyanate (MDI) was introduced into backbone chains of PDMS. The reaction process is shown in Figure 3. The amino groups at the end of PDMS molecules reacted with the isocyanate groups at the end of MDI to form a polar urea group. After the prepolymer was formed, the hydroxyl group of 1,4-butanediol (BDO) and MDI formed carbamate bonds and finally formed a long-chain modified PDMS.

On this basis, modified GO (iGO) modified by MDI was further introduced into MDI-PDMS-BDO. The isocyanate group at the edge of iGO acted as the reaction center and reacted with the amino group in the MDI-PDMS-BDO, forming a special structure with iGO as the cross-linking center.

3.3. Characterization of urea/urethane modified PDMS

Table 2 shows the GPC test results for modified PDMS with different PDMS/MDI/BDO ratios. The number average molecular weights of the synthesized MDI-PDMS-BDO samples with different hard segment contents were in the range of 40 000 to 70 000, and the molecular weight distribution was narrow, indicating that the length of MDI-PDMS-BDO were relatively uniform.

FTIR spectra in Figure 4a show the peaks at 1022 and 1088 cm^{-1} represent the characteristic vibrational peaks of Si–O–Si in the polysiloxane backbone, and the vibrational peak at 796 cm^{-1} is caused by the Si–C bond. The characteristic peaks of C=O bond in the urea group at 1650 cm^{-1} and C=O bond in carbamate
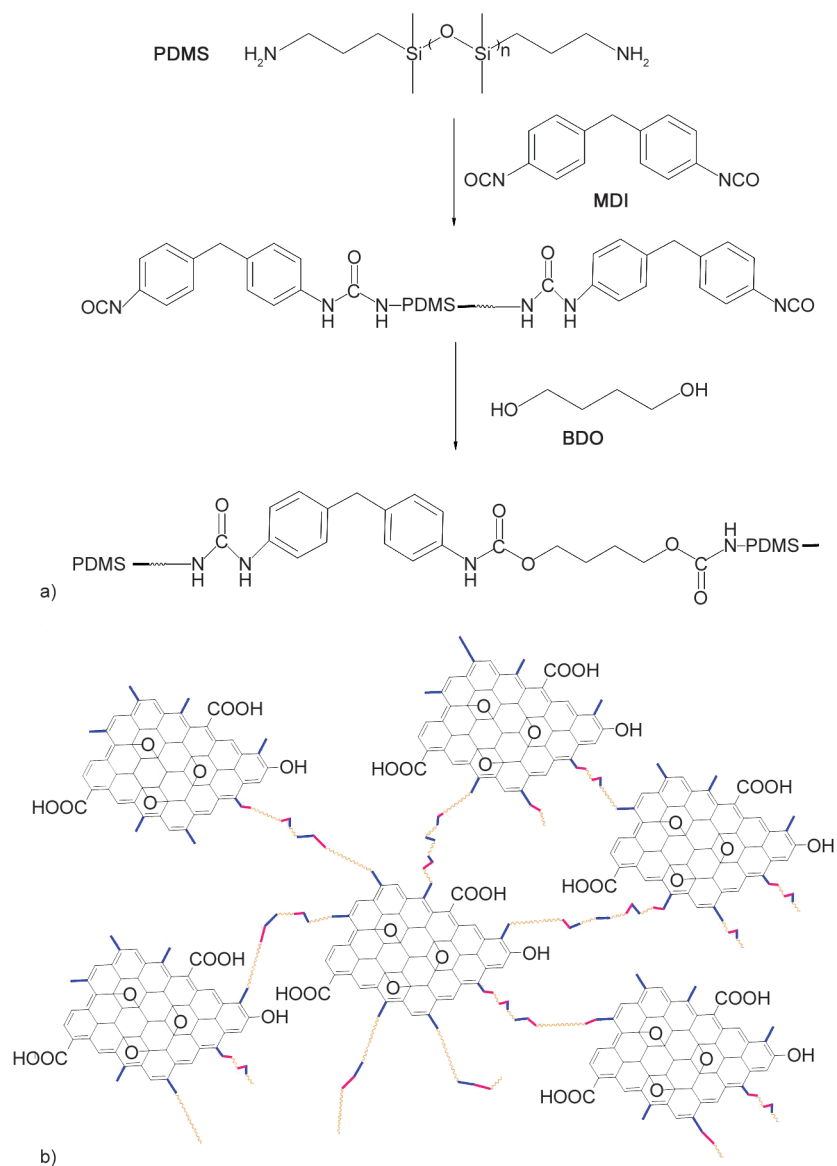
Figure 3. Synthesis mechanism of MDI-PDMS-BDO. a) The synthesis route of MDI-PDMS-BDO. b) The structure diagram of iGO/MDI-PDMS-BDO.

Table 2. Molecular weight and distribution of MDI-PDMS-BDO.

Sample	PDMS/MDI/BDO [mol ratio]	M_n^* [g/mol]	M_w^{**} [g/mol]	M_w/M_n
MDI-PDMS-BDO 1	1/2/1	46249	65134	1.41
MDI-PDMS-BDO 2	1/3/2	41610	52556	1.26
MDI-PDMS-BDO 3	1/4/3	67264	93826	1.39
MDI-PDMS-BDO 4	1/5/4	70430	94809	1.35
MDI-PDMS-BDO 5	1/6/5	67527	93764	1.38

$^*M_n$: number average molecular weight,
$^{**}M_w$: weight average molecular weight.

at 1710 cm^{-1} are proving the successful synthesis of urea-carbamate functionalized PDMS [25].

XRD patterns in Figure 4b show the ordered structures of the functionalized PDMS. The sharp diffusion peak shows the ordered structure in the functionalized PDMS, which was mostly formed by the regular arrangement of rigid groups such as urea and carbamate groups. However, the lesser dispersion peak is attributed to the disordered structure in the functionalized PDMS. The peak at 12.28° of the
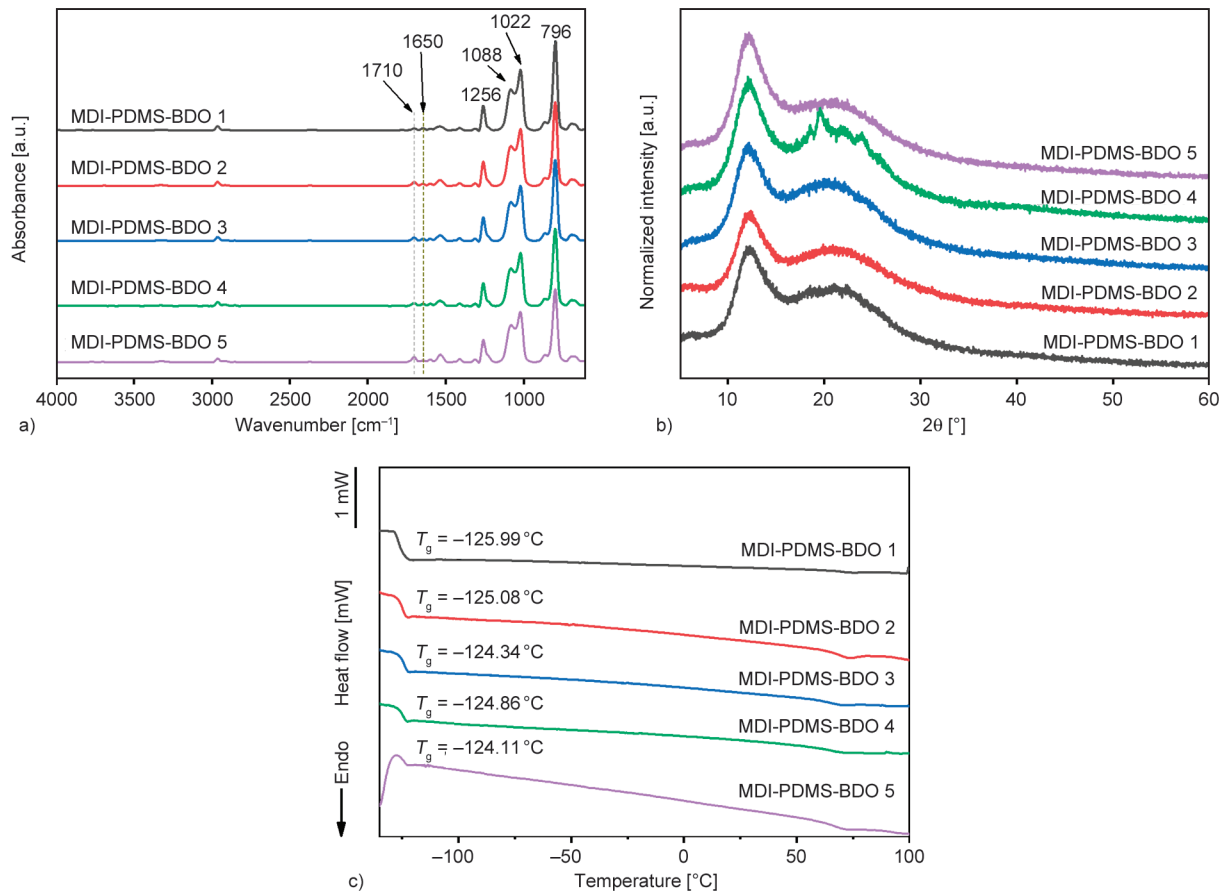
Figure 4. a) FTIR spectra, b) XRD patterns, c) DSC curves of MDI-PDMS-BDO.

functionalized PDMS became sharp with the increase in hard segment content while the peak height also increased slightly.

Hard segments are the source of ordered structures in PDMS. An ordered structure has an influence on the glass transition temperature and melting of functionalized PDMS. The DSC curves in Figure 4c show the T_g of functionalized PDMS for different carbamate contents. The increase in the carbamate proportion leads to a high T_g of the functionalized PDMS. This is because the ordered structure formed by the polar urea group and the carbamate group binds the flexible molecular chains of PDMS.

AFM images in Figure 5 show an obvious microphase separation structure in MDI-PDMS-BDO functionalized PDMS. The darker color represents the soft segment PDMS, forming a continuous phase. The brighter color represents the hard segment formed by the urea groups and the carbamate groups. They are uniformly distributed in the functionalized PDMS. With the increase of hard segment content, the Derjaguin-Muller-Toporov (DMT) modulus of functionalized PDMS is higher, and the ordered structure

formed by the urea group is shown to be easier to aggregate.

Furthermore, the sample of MDI-PDMS-BDO 5 with the high hard segment content was selected to react with different contents of iGO to form iGO/MDI-PDMS-BDO composites for further study.

3.4. Microstructure of iGO/MDI-PDMS-BDO composites

To form a filler network in functionalized PDMS, the –NCO in the iGO reacted with the amino group at the end of the MDI-PDMS-BDO to form a strong carbamate interface. GO sheets were tightly connected to the PDMS through these chemical bonds. Figure 6a shows that the peak of the –NCO group on the surface of iGO at 2265 cm^{-1} disappeared in the FTIR spectra of the composite. Obviously, the ratio of peak height at 1650 cm^{-1} for the urea group and 1710 cm^{-1} for the carbamate group in Figure 6b increased after the reaction, indicating that more urea groups were formed after the reaction between iGO and amino groups in the MDI-PDMS-BDO.
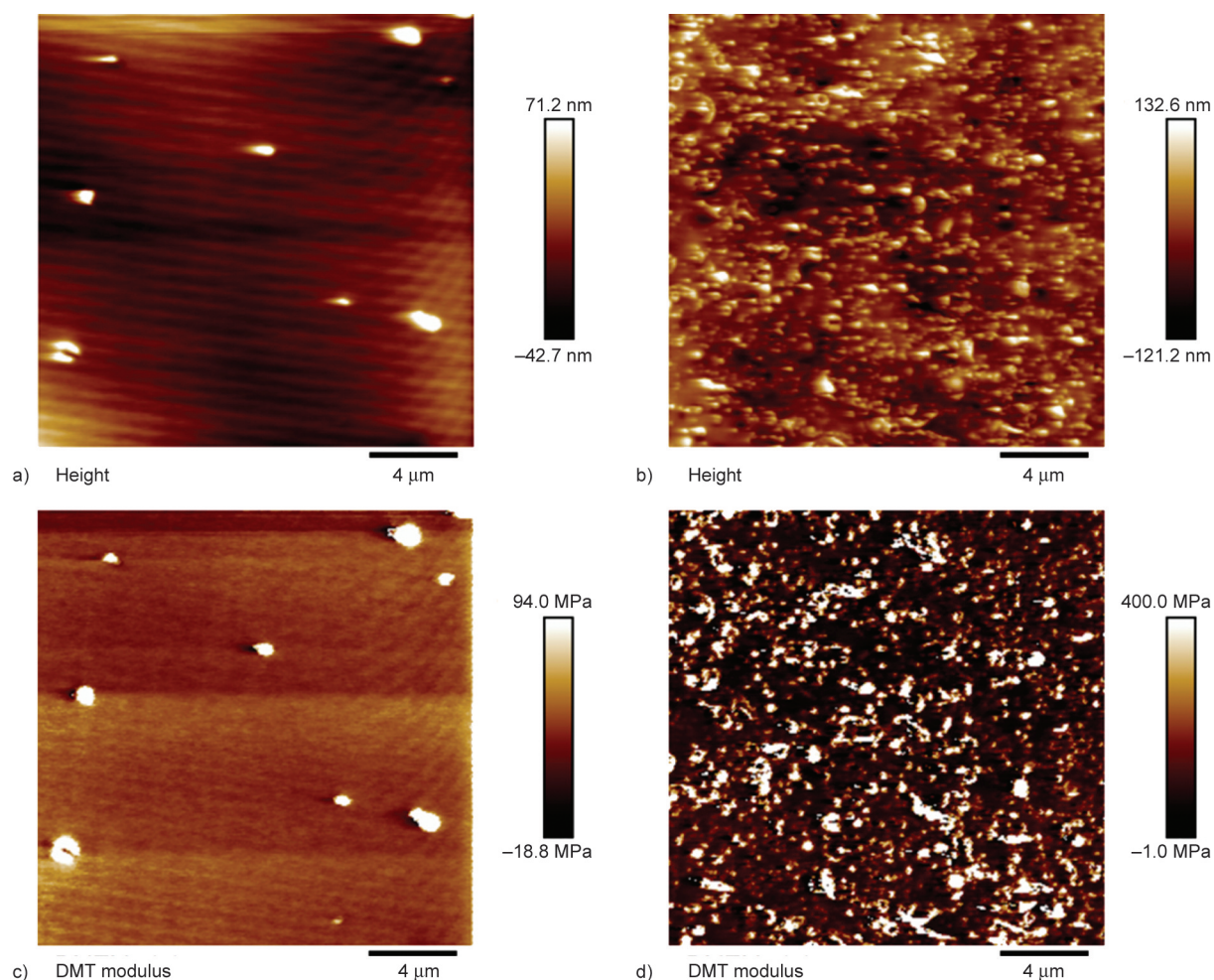
Figure 5. AFM images: a) height and c) modulus images of MDI-PDMS-BDO 1; b) height and d) modulus images of MDI-PDMS-BDO 5.

XRD patterns in Figure 6c show sharp diffraction peaks and diffusion peaks of a disordered structure, indicating that the addition of iGO had a significant influence on the ordered structure of the composites. Compared with the MDI-PDMS-BDO sample without iGO, the addition of iGO weakened the peak intensity of the ordered structure and affected the formation of the structure in the functional PDMS. This was attributed to iGO reacting with the PDMS chain through urea groups, resulting in a reduction in the content of hard segments.

A similar conclusion can also be drawn from the analysis of the DSC curve. Figure 6d shows the introduction of iGO leads to a decrease in T_g in the composite, compared with MDI-PDMS-BDO functionalized PDMS. Combined with the XRD patterns analysis, the ordered structure played a role in binding the flexible molecular chain in PDMS. When the formation of an ordered structure was affected by the addition of iGO, the flexible PDMS molecular chain was easily moved, leading to a decrease in T_g.

Moreover, with the increase of iGO content, the T_g of the composites were elevated, confirming the GO lamellar structure has a binding effect on the molecular chains of PDMS.

3.5. Morphologies of iGO/MDI-PDMS-BDO composites

SEM images in Figure 7 shows that the small circular hard particles are uniformly dispersed in the continuous phase of the PDMS. GO sheets were also wrapped in the functionalized PDMS matrix during the in-situ polymerization. No obvious boundaries between iGO and functionalized PDMS were found, indicating that a satisfactory interface was formed between iGO and the functionalized PDMS.

3.6. Mechanical properties of iGO/MDI-PDMS-BDO composites

Figure 8 and Table 3 show the stress-strain curves of iGO/MDI-PDMS-BDO composites. After the addition of iGO, the tensile strength of the composites
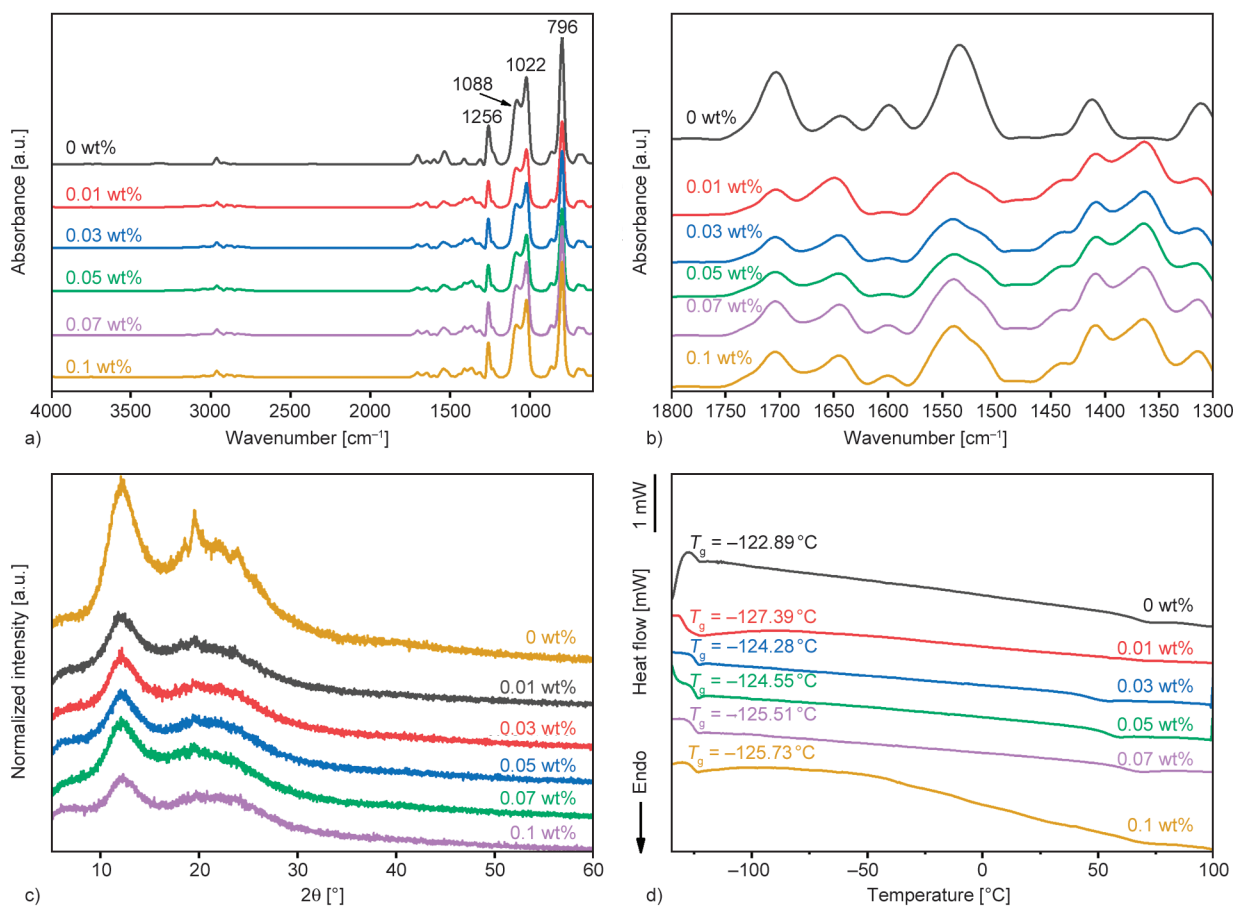
Figure 6. a) Full and b) local enlarged FTIR spectra with different wavenumber ranges; c) XRD patterns and d) DSC curves of iGO/MDI-PDMS-BDO composites.

greatly improved. The rigid structures in iGO/ MDI-PDMS-BDO composites formed by urea and urethane groups are beneficial to the improvement in mechanical properties of PDMS but also limit the slip and extension of the PDMS molecular chains, leading to the reduction in elongation at break. Additionally, an increase in iGO content increased the tensile strength of iGO/MDI-PDMS-BDO composites. When the iGO content was 0.07 wt%, the tensile strength of the composite reached a maximum value in the tests. When the iGO content was 0.1 wt%, the tensile strength decreased due to the decrease in the hard segment content.

3.7. Gas barrier properties of iGO/MDI-PDMS-BDO composites

The gas permeability values in Figure 9 show the gas barrier properties of iGO/MDI-PDMS-BDO composites were greatly improved when compared with pure PDMS. With the increase of iGO content, the gas permeability coefficient decreases gradually. When the iGO content was only 0.07 wt%, the gas

barrier property of the composite was increased by 64%, compared with that of pure PDMS. This improvement was also attributed to three differing rigid structures formed in the iGO/MDI-PDMS-BDO composites: (1) the ordered structure formed by the hard segments of the functionalized PDMS. (2) the enhanced interactions between MDI-PDMS-BDO molecules brought about by polar groups. (3) the rigid GO sheet and the strong urea-based interface formed between iGO and functionalized PDMS. These special structures make it more difficult for gas molecules to penetrate the material, prolonging the diffusion path and resulting in improved gas barrier properties.

In order to assess the contribution of this work, a comparison of the gas barrier properties in the reported rubber-based composites is summarized in Table 4. The gas permeability in this research was much lower than those of the silicone rubber filled with modified layered hydrotalcite (SR/Ca-Mg-Al LDH) [26], brominated butyl rubber (BIIR) [27] with dense side methyl groups, and mGO filled with
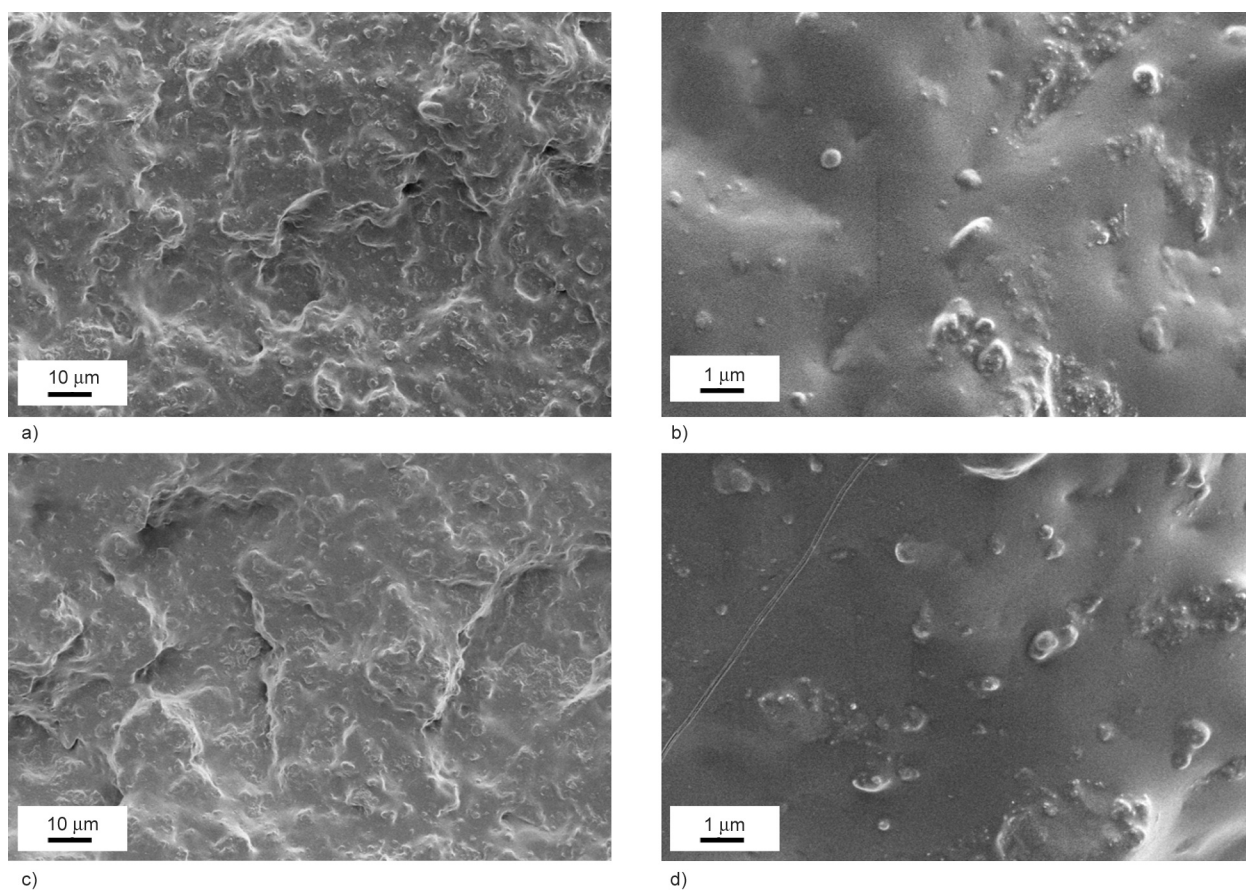
Figure 7. SEM images of iGO/MDI-PDMS-BDO composites: a) and b) represent the sample with 0.01 wt% iGO observed at the magnification of 2000× and 20 000×, respectively; c) and d) represent the sample with 0.07 wt% iGO observed at the magnification of 2000× and 20 000×, respectively.
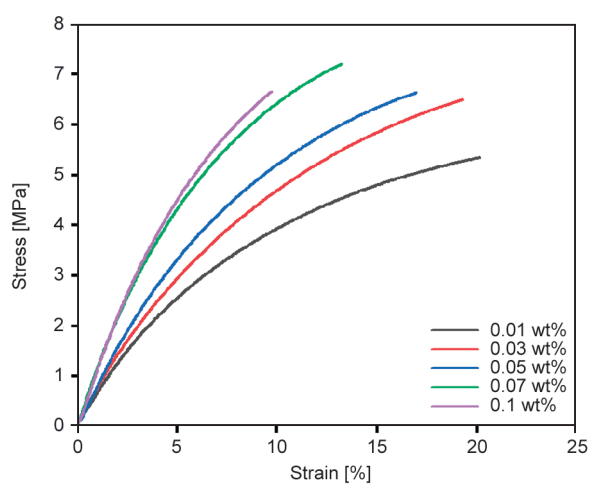

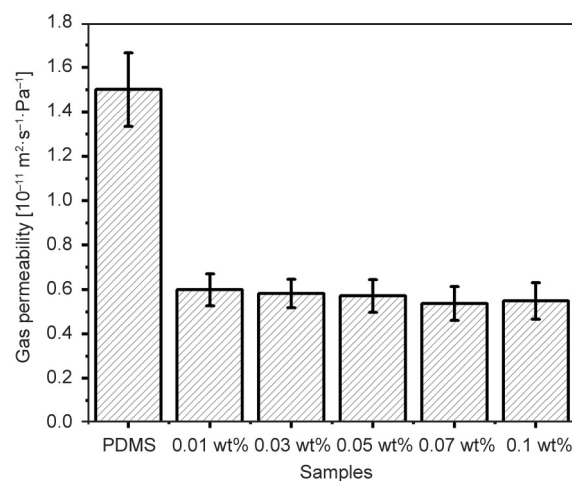**Figure 8.** Stress-strain curves of iGO/MDI-PDMS-BDO composites for a range of iGO content.

Figure 9. Gas permeability of iGO/MDI-PDMS-BDO composites for a range of iGO content.

Table 3. Mechanical properties of iGO/MDI-PDMS-BDO composites for a range of iGO content.

Sample		SiR	0.01 wt%	0.03 wt%	0.05 wt%	0.07 wt%	0.1 wt%
Tensile strength	[MPa]	0.4±0.1	5.4±0.2	6.5±0.2	6.7±0.4	7.2±0.3	6.6±0.2
Elongation at break	[%]	213±10	20±2	19±2	17±2	13±3	10±3
Hardness	[Shore A]	32±1	83±2	81±1	80±2	83±2	85±1

Table 4. Comparison between this work and other rubber based composites.

Sample	Composition	Gas permeability [$10^{-9}\cdot m^2\cdot s^{-1}\cdot Pa^{-1}$]	Reference
1	SR/Ca-Mg-Al LDH	5910	[26]
2	BIIR	0.332	[27]
3	TRL-mGO/BIIR	0.052	[27]
4	L-mGO/BIIR	0.031	[27]
5	This work	0.0054	

BIIR composites. The comparison indicates that the iGO/MDI-PDMS-BDO composites have excellent gas barrier properties due to the specially ordered structure, the enhanced interactions and the rigid GO sheet networks in the composites.

4. Conclusions

The MDI-PDMS-BDO functionalized PDMS was successfully prepared by the modification of PDMS chains with polar urea and carbamate. Accordingly, iGO/MDI-PDMS-BDO PDMS composites were prepared by *in-situ* polymerization with modified GO as the cross-linking center. The ordered structure was formed by hard segments of the MDI-PDMS-BDO functionalized PDMS. A strong urea-based interface was also formed between iGO and functionalized PDMS. iGO became the cross-linking center in the iGO/MDI-PDMS-BDO composites. The introduction of polar groups, hard segments and iGO sheets enabled the tensile strength of iGO/MDI-PDMS-BDO composites to increase to 7.2 MPa. More importantly, the gas barrier property achieved using iGO/MDI-PDMS-BDO composites was improved by 64% compared with that of pure PDMS when the iGO content was 0.07 wt%.

Acknowledgements

References
[1] Xu Z., Xiao Y., Zhou Y., Hong Y., Lai Q., Wang C., Bian H., Li W.: Preparation of high-performance natural rubber composites: Plasma-foaming agent-modified kaolin and flash-drying technology. Journal of Applied Polymer Science, **140**, e54103 (2023). https://doi.org/10.1002/app.54103

[2] Wang L., Zhang J., Sun Y., Zhang T., Wang L., Wang J., Liang Y., Hao M., Fu Q.: Green preparation and enhanced gas barrier property of rubber nanocomposite film based on graphene oxide-induced chemical cross-linking. Polymer, **225**, 123756 (2021). https://doi.org/10.1016/j.polymer.2021.123756

[3] Raju A. T., Parathodika A. R., Naskar K.: Evaluation of the barrier and mechanical characteristics of bromobutyl rubber-containing blends for use in inner liner of automotive tires. Journal of Applied Polymer Science, **140**, e54505 (2023). https://doi.org/10.1002/app.54505

[4] Prignon M., van Moeseke G.: Factors influencing airtightness and airtightness predictive models: A literature review. Energy and Buildings, **146**, 87–97 (2017). https://doi.org/10.1016/j.enbuild.2017.04.062

[5] Chen J., Ding N., Li Z., Wang W.: Organic polymer materials in the space environment. Progress in Aerospace Sciences, **83**, 37–56 (2016). https://doi.org/10.1016/j.paerosci.2016.02.002

[6] Gouzman I., Girshevitz O., Grossman E., Eliaz N., Sukenik C.: Thin film oxide barrier layers: Protection of kapton from space environment by liquid phase deposition of titanium oxide. ACS Applied Materials and Interfaces, **2**, 1835–1843 (2010). https://doi.org/10.1021/am100113t

[7] Tong Q. Y., Fountain G., Enquist P.: Room temperature SiO_2/SiO_2 covalent bonding. Applied Physics Letters, **89**, 042110 (2006). https://doi.org/10.1063/1.2240232

[8] Xu Q., Pang M., Zhu L., Zhang Y., Feng S.: Mechanical properties of silicone rubber composed of diverse vinyl content silicone gums blending. Materials and Design, **31**, 4083–4087 (2010). https://doi.org/10.1016/j.matdes.2010.04.052

[9] Abd-El Salam M. H., El-Gamal S., Mohsen M., Abd El-Maqsoud D. M.: Effect of conductive fillers on the cyclic stress-strain and nano-scale free volume properties of silicone rubber. Chinese Journal of Polymer Science, **32**, 558–567 (2014). https://doi.org/10.1007/s10118-014-1428-7

[10] Cai F., You G., Zhao X., Hu H., Wu S.: The relationship between specific structure and gas permeability of bromobutyl rubber: A combination of experiments and molecular simulations. Macromolecular Theory and Simulations, **28**, 1900025 (2019). https://doi.org/10.1002/mats.201900025

[11] Sun H., Liu X., Yu B., Feng Z., Ning N., Hu G-H., Tian M., Zhang L.: Simultaneously improved dielectric and mechanical properties of silicone elastomer by designing a dual crosslinking network. Polymer Chemistry, **10**, 633–645 (2019). https://doi.org/10.1039/C8PY01763H

[12] Riehle N., Thude S., Götz T., Kandelbauer A., Thanos S., Tovar G. E. M., Lorenz G.: Influence of PDMS molecular weight on transparency and mechanical properties of soft polysiloxane-urea-elastomers for intraocular lens application. European Polymer Journal, **101**, 190–201 (2018).
https://doi.org/10.1016/j.eurpolymj.2018.02.029

[13] Zhang H., Liang Y., Wang P., Zhang D.: Design of slippery organogel layer with room-temperature self-healing property for marine anti-fouling application. Progress in Organic Coatings, **132**, 132–138 (2019).
https://doi.org/10.1016/j.porgcoat.2019.03.020

[14] Liu Y., Zhu D., Sun J., Wu Y., Gao C.: A new cross-linked system of silicone rubber based on silicone-polyurea block copolymer. Polymers for Advanced Technologies, **29**, 2064–2071 (2018).
https://doi.org/10.1002/pat.4314

[15] Zang W., Liu X., Li J., Jiang Y., Yu B., Zou H., Ning N., Tian M., Zhang L.: Conductive, self-healing and recyclable electrodes for dielectric elastomer generator with high energy density. Chemical Engineering Journal, **429**, 132258 (2022).
https://doi.org/10.1016/j.cej.2021.132258

[16] Song Y., Yu J., Yu L., Alam F. E., Dai W., Li C., Jiang N.: Enhancing the thermal, electrical, and mechanical properties of silicone rubber by addition of graphene nanoplatelets. Materials and Design, **88**, 950–957 (2015).
https://doi.org/10.1016/j.matdes.2015.09.064

[17] Sarath P., Reghunath R., Thomas S., Haponiuk J. T., George S. C.: An investigation on the tribological and mechanical properties of silicone rubber/graphite composites. Journal of Composite Materials, **55**, 3827–3838 (2021).
https://doi.org/10.1177/00219983211031634

[18] She X., He C., Peng Z., Kong L.: Molecular-level dispersion of graphene into epoxidized natural rubber: Morphology, interfacial interaction and mechanical reinforcement. Polymer, **55**, 6803–6810 (2014).
https://doi.org/10.1016/j.polymer.2014.10.054

[19] Bernard C., Goodwin D. G., Gu X., Celina M., Nyden M., Jacobs D., Sung L., Nguyen T.: Graphene oxide/waterborne polyurethane nanocoatings: Effects of graphene oxide content on performance properties. Journal of Coatings Technology and Research, **17**, 255–269 (2020).
https://doi.org/10.1007/s11998-019-00267-6

[20] Zheng L., Wang D., Xu Z., Zhang L., Liu L., Wen S.: High barrier properties against sulfur mustard of graphene oxide/butyl rubber composites. Composites Science and Technology, **170**, 141–147 (2019).
https://doi.org/10.1016/j.compscitech.2018.12.002

[21] Hummers W. S., Offeman R. E.: Preparation of graphitic oxide. Journal of the American Chemical Society, **80**, 1339–1339 (1958).
https://doi.org/10.1021/ja01539a017

[22] Yoon S. H., Park J. H., Kim E. Y., Kim B. K.: Preparations and properties of waterborne polyurethane/allyl isocyanated-modified graphene oxide nanocomposites. Colloid and Polymer Science, **289**, 1809–1814 (2011).
https://doi.org/10.1007/s00396-011-2498-5

[23] Li Y., Tian H., Zhang J., Zou W., Wang H., Du Z., Zhang C.: Fabrication and properties of rigid polyurethane nanocomposite foams with functional isocyanate modified graphene oxide. Polymer Composites, **41**, 5126–5134 (2020).
https://doi.org/10.1002/pc.25780

[24] Stobinski L., Lesiak B., Malolepszy A., Mazurkiewicz M., Mierzwa B., Zemek J., Jiricek P., Bieloshapka I.: Graphene oxide and reduced graphene oxide studied by the XRD, TEM and electron spectroscopy methods. Journal of Electron Spectroscopy Related Phenomena, **195**, 145–154 (2014).
https://doi.org/10.1016/j.elspec.2014.07.003

[25] Wittmer A., Brinkmann A., Stenzel V., Hartwig A., Koschek K.: Moisture-mediated intrinsic self-healing of modified polyurethane urea polymers. Journal of Polymer Science Part A: Polymer Chemistry, **56**, 537–548 (2018).
https://doi.org/10.1002/pola.28925

[26] Li D., Lin Q., Liu L., Song X., Wang Z., Sun X., Xue Y., Fu Y., Shi Y., Li Z., Gui X., Xu K.: Intercalation of silsesquioxane surfactant in layered double hydroxide for silicone rubber composites: Enhancing interfacial interactions toward improvement of mechanical, thermal, and gas barrier properties. Polymer Composites, **44**, 8389–8402 (2023).
https://doi.org/10.1002/pc.27705

[27] Yang S., Wu H., Li C., Xiong Y., Guo S.: Constructing oriented two-dimensional large-sized modified graphene oxide barrier walls in brominated butyl rubber to achieve excellent gas barrier properties. ACS Applied Materials and Interfaces, **12**, 3976–3983 (2020).
https://doi.org/10.1021/acsami.9b19802